ACS Catalysis

Research Article

pubs.acs.org/acscatalysis

Isolated Fe^{II} on Silica As a Selective Propane Dehydrogenation Catalyst

Bo Hu,[†] Neil M. Schweitzer,[‡] Guanghui Zhang,[‡,§] Steven J. Kraft,[‡] David J. Childers,[∥] Michael P. Lanci,[‡] Jeffrey T. Miller,*[,‡] and Adam S. Hock*[,†,‡]

[†]Department of Chemistry, Illinois Institute of Technology, Chicago, Illinois 60616, United States

[‡]Chemical Sciences and Engineering Division, Argonne National Laboratory, Argonne, Illinois 60439, United States

[§]College of Chemistry and Molecular Sciences, Wuhan University, Wuhan, 430072, People's Republic of China

[∥]Department of Chemical Engineering, University of Illinois at Chicago, Chicago, Illinois 60607, United States

Supporting Information

ABSTRACT: We report a comparative study of isolated Fe^{II}, iron oxide particles, and metallic nanoparticles on silica for non-oxidative propane dehydrogenation. It was found that the most selective catalyst was an isolated Fe^{II} species on silica prepared by grafting the open cyclopentadienide iron complex, bis(2,4-dimethyl-1,3-pentadienide) iron(II) or $Fe(o\mathrm{Cp})_2$. The grafting and evolution of the surface species was elucidated by ^{1}H NMR, diffuse reflectance infrared Fourier transform spectroscopy and X-ray absorption spectroscopies. The oxidation state and local structure of surface Fe were characterized by X-ray absorption near-edge structure (XANES) and extended X-ray absorption fine structure. The initial grafting of iron proceeds by one surface hydroxyl Si−OH reacting with $Fe(o\mathrm{Cp})_2$ to release one diene ligand (oCpH), generating a SiO_2-bound $Fe^{II}(o\mathrm{Cp})$ species, **1-Fe*o*Cp**. Subsequent treatment with H_2 at 400 °C leads to loss of the remaining diene ligand and formation of nanosized iron oxide clusters, **1-C**. Dispersion of these Fe oxide clusters occurs at 650 °C, forming an isolated, ligand-free Fe^{II} on silica, **1-Fe^{II}**, which is catalytically active and highly selective (~99%) for propane dehydrogenation to propene. Under reaction conditions, there is no evidence of metallic Fe by in situ XANES. For comparison, metallic Fe nanoparticles, **2-NP-Fe^0**, were independently prepared by grafting $Fe[N(SiMe_3)_2]_2$ onto silica, **2-FeN***, and reducing it at 650 °C in H_2. The Fe NPs were highly active for propane conversion but showed poor selectivity (~14%) to propene. Independently prepared Fe oxide clusters on silica display a low activity. The sum of these results suggests that selective propane dehydrogenation occurs at isolated Fe^{II} sites.

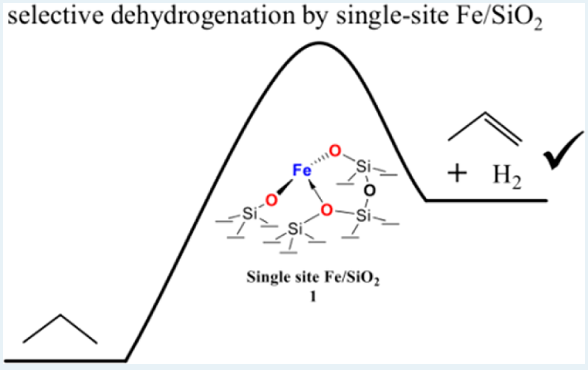

KEYWORDS: *isolated Fe catalysts, propane dehydrogenation, Fe nanoparticles on silica, dehydrogenation catalyst, Fe XANES, EXAFS*

INTRODUCTION

Selective activation of sp^3 C−H bonds is a critical component for alkane transformations. It is especially challenging to control C−H versus C−C cleavage when performing endothermic reactions, such as non-oxidative dehydrogenation of alkanes to the alkene and hydrogen. The transformation of propane to propene and hydrogen becomes thermodynamically favorable above temperatures of ~400 °C; however the competing reaction to cleave a C−C bond to yield methane and ethene becomes favorable at 200 °C. Thus, both kinetic and thermodynamic considerations make this reaction particularly challenging. Nonetheless, this reaction is performed commercially using Cr- and Sn-modified Pt catalysts, with catalyst regeneration to remove carbon deposits due to unselective C−C and C−H activation forming a key engineering component. Bulk oxides, such as Ga_2O_3, are also active for alkane dehydrogenation; however, the rates are low, and these catalysts also deactivate by forming coke.[1−4] Isolated metal ions in the zeolite framework or ion-exchanged into zeolites, for example, Zn(II),[5,6] Co(II),[7,8] and Ga(III),[5,6,9,10] have also been suggested as catalysts for dehydrogenation of alkanes to olefins; however, the residual protons lead to secondary reactions forming a variety of alkanes, alkenes, and aromatics.[11,12] Nevertheless, these results suggest that the isolated metal ions may be promising catalytic species for selective alkane dehydrogenation.

We have found that the catalytic properties of these isolated ions can be studied independently if they are synthesized free of Brønsted acid sites on SiO_2. Furthermore, we have demonstrated that silica-supported, well-defined isolated Zn(II)[13] and Co(II)[14] catalysts are catalytically active and selective for propane dehydrogenation at 550 °C or even at 650 °C in some

Received: February 5, 2015
Revised: April 8, 2015
Published: April 17, 2015

DOI: 10.1021/acscatal.5b00248
ACS Catal. 2015, 5, 3494−3503

cases. At this temperature, the thermodynamics favor dehydrogenation and C−C cleavage reactions, but we observe very high kinetic selectivities to the dehydrogenation products. We believe that Si vacancies on the SiO_2 surface can behave as a "tetrahedral enforcer" (cf. scorpionates[15] and other related ligands[16−21]), stabilizing low coordinate metal centers toward reduction to metallic phases or aggregation into metal oxide clusters.

The synthesis of our zinc and cobalt catalysts is performed using the stable ammonia coordination complexes in water, followed by thermally dissociating the ammonia ligands. This approach is not viable for iron because it forms oxides rapidly in basic aqueous solution. Thus, we have adopted organometallic precursors for the formation of isolated Fe^{II} species on silica. Surface organometallic chemistry of this type is a powerful way to prepare well defined catalytic species by protonolysis of reactive metal ligands with hydroxyl groups of the support, for example, SiO_2 and Al_2O_3.[22−27] Several approaches to isolated surface catalysts exist. Some supporting ligands can be retained, such as in the case of Mo and W imido alkylidene metathesis catalysts studied by Schrock, Copéret, and co-workers,[24,28−30] or all non-oxygen ligands can be removed, as the thermolytic synthesis routes Tilley has pioneered.[31−35] Finally, metals can be dispersed using chelating additives, such as ethylene-(diamine)tetraacetic acid has been used by Notestein and co-workers.[36]

In the case of iron, Tilley et al. prepared Fe^{3+} catalysts on SiO_2 by grafting $Fe[OSi(Ot\text{-}Bu)_3]_3$ on SBA-15, followed by calcination to remove the remaining organic groups. Notestein et al. used the iron ethylene(diamine)tetraacetic acid (EDTA) complex to prepare highly-dispersed iron species on SiO_2 surface and also removed the EDTA via calcination. In both cases, the resulting surface iron species were able to catalyze oxidation of alkanes, alkene, and arenes with hydroperoxide with good selectivity.[31] Isolated Fe species incorporated into the matrix of silicates also exhibit interesting catalytic properties. By incorporating isolated Fe in the framework of a zeolite, the resulting Fe-ZSM5 was demonstrated by Lobo et al. to be catalytically active for selective propane transformations.[37] In addition, isolated Fe^{III} in the matrix of silicate was also successfully prepared by Tušar et al. through two-step solvothermal synthesis.[38,39] Such Fe silicate material was studied as an efficient adsorbent and catalyst for toluene oxidation. In both Fe systems, redox of isolated Fe^{II}/Fe^{III} was postulated to be critical for their catalytic performance.

Herein, we report the synthesis, characterization and catalytic properties for propane dehydrogenation by a well-defined, isolated Fe^{II}/SiO_2, **1-Fe^{II}**, and a comparison with metallic nanoparticles (**2-NP-Fe^0**) and oxides clusters. The surface chemistry utilized to prepare isolated Fe species uses bis(2,4-dimethyl-1,3-pentadienide) iron(II), $Fe^{II}(o\text{Cp})_2$,[40,41] which we have previously used as an atomic layer deposition precursor to Fe_2O_3 and Fe_3O_4.[42] The structure of the Fe species at different stages of the synthesis was elucidated by ^{1}H NMR, diffuse reflectance infrared Fourier transform spectroscopy (DRIFTS), in situ X-ray absorption near-edge structure (XANES) and extended X-ray absorption fine structure (EXAFS). The catalytically active species is an isolated, three-coordinate Fe(II) silicate. This is in contrast to the chemistry of $Fe[N(SiMe_3)_3]_2$[43] on silica, **2-FeN***, which reduces to metallic nanoparticles, **2-NP-Fe^0** upon reduction at 650 °C in hydrogen. We demonstrate that although Fe NPs are highly active, propane is nonselectively converted to methane/ethylene, and a rapid coke formation was observed. Silica-supported iron oxide clusters were also prepared and found to have little activity. The differences in catalytic activity and selectivity indicate that isolated Fe^{II} on silica is the active site for selective propane dehydrogenation.

EXPERIMENTAL SECTION

All synthetic operation is performed under a N_2 atmosphere in the glovebox or using Schlenk techniques. All nonaqueous, air-free solvents are purified and dried by solvent system. The silica (Davisil 646, 35−60 mesh, Sigma-Aldrich) was dried under vacuum at 200 °C down to 5 milli-Torr and was kept in the glovebox under nitrogen atmosphere. Other chemicals are all reagent grade or above, and no further purification was performed. Elemental analysis was determined by Galbraith Laboratories, Inc. (Knoxville, TN)

Bis(2,4-dimethyl-1,3-pentadienide) Iron(II) (Fe(o-Cp)$_2$).[41,42,44] $MgBr_2$ (3 g; 16.3 mmol) was dissolved in 40 mL of THF in a 200 mL round-bottom flask, and it was kept cold to −78 °C. Potassium 2,4-dimethyl-pentadienide (2.17 g; 16.2 mmol) was dissolved in 30 mL of THF and was cooled to −78 °C. The solution of potassium pentadienide was added dropwise to the $MgBr_2$ THF solution when they were cold (at −78 °C). The reaction mixture was stirred for 2 h at room temperature and was added dropwise into 1.03 g of anhydrous $FeCl_2$ (8.1 mmol) THF solution at −78 °C. The mixture was stirred for another 3 h at room temperature, yielding a deep red solution. Then the THF was removed in vacuum, and the bis(2,4-dimethyl-1,3-pentadienide) iron(II) ($Fe(o\text{-}Cp)_2$) was extracted with pentane. The filtered extraction solution was evacuated to remove the pentane to yield 0.84g (42.2%) of product. ^{1}H NMR (500 MHz, C_6D_6): δ_H 4.36 (s, 1 H), 2.66 (s, 2 H), 1.83 (s, 6 H), 0.29 (s, 2 H)

Grafting Bis(2,4-dimethyl-1,3-pentadienide) Iron(II) onto Silica (1-FeoCp). A solution of 0.176 g (0.72 mmol) of 2,4-dimethyl-1,3-pentadienide iron(II) in 10 mL of hexanes was added to 2 g of dry silica in a 50 mL flask under N_2. The mixture was stirred for 3 h at room temperature, and the resulting solid material was filtered and washed with pentane. The as-prepared material was dried in vacuum to obtain a red-orange solid (2.01 g, 98%). Anal. found: Fe, 1.11.

Bis[bis(trimethylsilyl)amide] Iron(II) (Fe[N(SiMe$_3$)$_2$]$_2$).[43,45] $Li[N(SiMe_3)_2]$ (1.32 g; 7.9 mmol) was dissolved in Et_2O and was kept cold in the freezer (−30 °C). The cold lithium salt solution was added into a suspension of 500 mg of anhydrous $FeCl_2$ (3.9 mmol) in Et_2O at −30 °C. The reaction was warmed to room temperature and was stirred overnight. The Et_2O was removed in vacuum, and the Fe compound was extracted with hexanes. The solution was filtered, and the solvent was removed in vacuum to obtain 1.35 g (92%) of the product. ^{1}H NMR (500 MHz, tol-d_8): δ_H 65.58 (s, br, 36 H).

Grafting Fe[N(SiMe$_3$)$_2$]$_2$ onto Silica (2-FeN*). Bis[bis-(trimethylsilyl)amide] iron(II) (0.134 g, 0.36 mmol) hexanes (10 mL) solution was added into a dry silica (1 g) hexanes slurry in a 20 mL vail. The mixture was stirred for 1 h at room temperature. The resulting solid was filtered and dried in vacuum for an hour to get a greenish solid (0.98 g). Anal. found: Fe, 1.83.

Reduction of Fe[N(SiMe$_3$)$_2$]$_2$/SiO$_2$. The $Fe[N(SiMe_3)_2]_2/SiO_2$ (**2-FeN***) sample (1 g) was loaded into a quartz reactor under nitrogen atmosphere. The whole gas line was purged with 4% hydrogen (50 mL/min) with helium for 10 min, and

DOI: 10.1021/acscatal.5b00248
ACS Catal. 2015, 5, 3494−3503

then the hydrogen gas was purged through the reactor for another 5 min at room temperature. The temperature of the reactor was set to 650 °C and held for 10 min with the constant hydrogen gas flowing rate (4% in helium, 50 mL/min). Metallic Fe nanoparticles were obtained after hydrogen reduction.

Fe_2O_3 Clusters on SiO_2. Fe oxide on silica was synthesized using the incipient wetness impregnation methodology. Iron nitrate ($Fe(NO_3)_3 \cdot 9H_2O$, 7.28 g; Aldrich) was dissolved in 20 mL of deionized water, and the solution was added to 20 g of silica dropwise while stirring to mix them well. The resulting wet powder was dried overnight at 125 °C and subsequently calcined at 300 °C in air for 3 h. Anal. found: Fe, 4.4.

Catalyst Testing. The catalyst performance testing was conducted in a vertical, quartz tube reactor equipped with mass flow controllers, and the products were determined by online gas chromatography (50 m GS-alumina capillary column). Approximately 1 g of catalyst was packed in the glovebox under air-free atmosphere and was supported on quartz wool with an internal thermocouple placed at the top of the catalyst bed. The reactor was well sealed to keep the catalyst air-free during the whole catalytic testing. Initially, the catalyst was purged with H_2 (4% in helium, Airgas USA, LLC) or Ar (Airgas USA, LLC), which had been further purified with an oxygen trap, at 50 mL/min at room temperature for 5 min, then the reactor was heated to 650 °C for dehydrogenation. The reaction mixture was 3% propane/Ar at 55 mL/min or a contact time of 3 s for propane dehydrogenation. Product composition was determined by gas calibration standards and analyzed by a flame ionization detector (FID) using H_2 (99.999%, Airgas USA, LLC) and air (<2 ppm of H_2O, Airgas USA, LLC).

XANES and EXAFS Measurements. In situ XANES and EXAFS measurements at the Fe K-edge (7.112 keV) were conducted on the bending magnet beamline of the Materials Research Collaborative Access Team (MRCAT, 10-BM) at the Advanced Photon Source (APS), Argonne National Laboratory. Ionization chambers were optimized at the midpoint of the Fe spectrum for the maximum current with linear response (~10^{10} photons detected per second) using 35% He in N_2 (15% absorption) in the incident X-ray detector and a mixture of ~17% Ar in N_2 (70% absorption) in the transmission X-ray detector. A third detector in the series simultaneously collected an Fe foil reference spectrum with each measurement for energy calibration. A cryogenically cooled double-crystal Si(111) monochromator was used and detuned to 50% to minimize the presence of harmonics. The X-ray beam was 0.5 × 1.5 mm, and data were collected in transmission geometry in 10 min in step scan mode. The catalyst was pressed into a 4 mm self-supporting wafer and placed in a stainless steel holder. The reactor consisted of a straight quartz tube (1 in. o.d., 10 in. length) with an Ultra-Torr fitting equipped with shut-off valves. At both ends of the reactor were Kapton windows sealed with O-rings. The reactor has an internal thermocouple at the sample that controls the clam shell furnace. The as-prepared catalyst was loaded into a glovebox, and measurements were obtained at room temperature in the absence of air and water. The catalyst was treated for 30 min in flowing H_2 at 400 and 650 °C and in propane/He at 650 °C. After treatment at elevated temperature, the catalysts were cooled in the flowing gas and measured at room temperature without exposure to air.

X-ray absorption analysis of the Fe K-edge XANES energy was determined from the inflection point of the leading edge, by determination of the energy of the maximum in the first peak of the first derivative. EXAFS fits of the Fe/SiO_2 catalysts were determined from experimental phase shift and backscattering amplitudes, which were obtained from the $Fe(acac)_3$ (6 Fe−O at 1.99 Å). Standard procedures based on WINXAS 3.1 software were used to fit the X-ray absorption spectroscopies (XAS) data. The EXAFS coordination parameters were obtained by a least-squares fit in *R*-space of the first-shell, nearest neighbor, k^2-weighted Fourier transform data from Δk = 2.6−10.6 $Å^{-1}$.

Scanning Transmission Electron Microscopy (STEM). The STEM micrographs were obtained at the University of Illinois at Chicago, UIC's Research Resources Center facility using a JEOL 3010 Materials Science TEM, a 300 kV transmission electron microscope with LaB6 electron source. Samples were dispersed into an isopropyl alcohol solution and sonicated for 20 min. A drop of the solution was added to a holey-carbon copper grid and dried under a heat lamp for 20 min. Once the grid was dried, the sample was placed in a JEOL JEE-4X vacuum evaporator, and an overcoat of carbon was applied. Images were taken using the Gatan Orius SC200 CCD camera, and the particle size was counted using the Particule2 program. When particles were present, a minimum of 50 particles were counted to get an accurate representation of the particle size distribution.

DRIFTS Measurement. Infrared (IR) spectra were collected in a glovebox under N_2 atmosphere using a Bruker Alpha FTIR spectrometer (Bruker Optics, Billerica, MA) with a DRIFTS module. Spectra at 4 cm^{-1} resolution were obtained in absorbance mode over the 400−4000 cm^{-1} range. All IR data were analyzed using OPUS (v7.0, Bruker Optics, Billerica, MA) software.

Solution NMR Measurement. Solution ^1H NMR spectra were recorded using a Bruker UltraShield 500 MHz spectrometer. All data were analyzed using TopSpin v3.1 (Bruker BioSpin, Billerica, MA).

RESULTS AND DISCUSSION

Synthesis and Characterizations of Fe/SiO_2 Catalysts (isolated Fe^{II}/SiO_2, Metallic Fe^0 Nanoparticles and Fe Oxide Clusters). Our choice for grafting Fe^{II} onto silica (dried at 200 °C) is the open metallocene, bis(2,4-dimethylpentadienyl)iron ($Fe(oCp)_2$). The precursor is stable at ambient temperature under inert atmosphere, but the noncyclic diene ligand can be protonated by surface hydroxyl groups, resulting in isolated Fe sites on silica (**1-Fe*o*Cp**) that retains one *o*Cp ligand, as shown in Scheme 1. One equivalent of free diene ligand versus external standard was detected by ^1H NMR. In addition, the infrared spectrum of **1-Fe*o*Cp** shows C−H stretching around 3000 cm^{-1} (Figure 1) due to the remaining pentadienyl ligand. A loss of IR signal was also observed at 3740 cm^{-1} compared wtih SiO_2 due to the consumption of isolated surface hydroxyl groups.

Scheme 1. Grafting of $Fe(oCp)_2$ Precursor onto Silica To Form 1-Fe*o*Cp

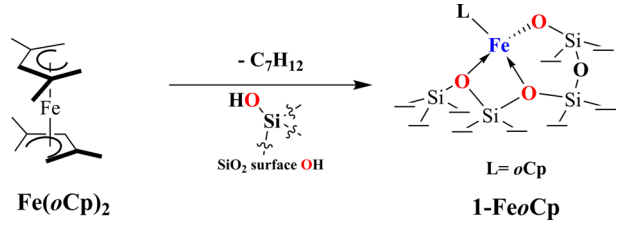

DOI: 10.1021/acscatal.5b00248
ACS Catal. 2015, 5, 3494−3503

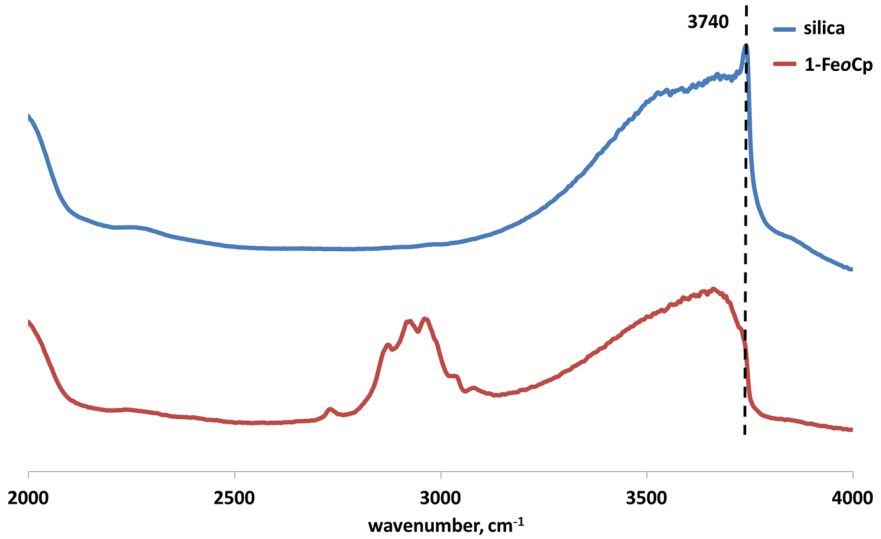

Figure 1. Diffuse reflectance infrared Fourier transform spectroscopy (DRIFTS) spectra of **1-Fe*o*Cp** (bottom) and silica (top).

The iron bis(hexamethyl)disilazide complex $Fe[N(SiMe_3)_2]_2$ also reacts with SiO_2 to release $HN(SiMe_3)_2$ to prepare **2-FeN*** (Scheme 2). However, the amount of released $HN(SiMe_3)_2$

Scheme 2. Grafting of Iron (II) Precursor ($Fe[N(SiMe_3)_2]_2$) onto Silica To Form 2-FeN*

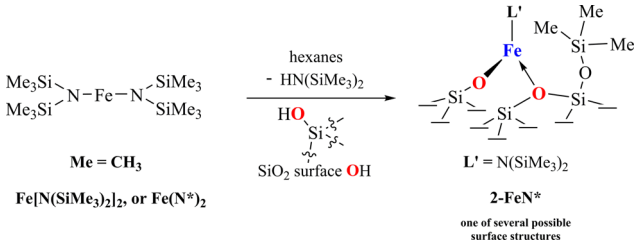

could not be accurately quantitated because of the competing reaction of the amine with surface Si−OH groups to form Si−O−$SiMe_3$ moieties. Diffuse reflectance infrared Fourier transform spectroscopy (DRIFTS) spectrum of **2-FeN*** shows the retention of C−H stretches consistent with the $SiMe_3$ groups, Figure 2. Moreover, the disappearance of the hydroxyl signal (compared with silica spectrum) at 3740 cm^{-1} indicates that $Fe[N(SiMe_3)_2]_2$ is chemically grafted onto silica by reacting with isolated ≡SiOH on the surface.

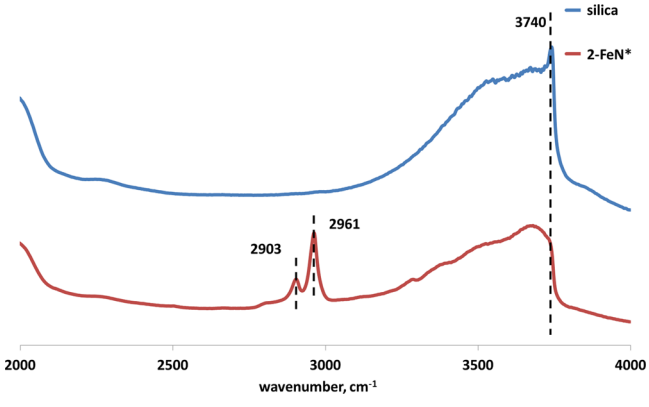

Figure 2. DRIFT spectra of **2-FeN*** (bottom) and silica (top).

The formal oxidation state and the local coordination geometry of Fe in **1-Fe*o*Cp** and **2-FeN*** were determined by XANES and EXAFS spectroscopies, respectively. The pre-edge energy of the 3d transition metal ions is indicative of the formal oxidation state in XANES spectra. The XANES spectrum of **1-Fe*o*Cp** is shown in Figure 3. The pre-edge energy of both **1-Fe*o*Cp** and **2-FeN*** are 7112.9 eV, as listed in Table 1, consistent with Fe^{II} (see Table S1 for the pre-edge energies of Fe(II) and Fe(III) reference compounds). One benefit of XAS methods is that the material can be examined under reaction conditions to follow the evolution of metal species during catalysis. We will consider the behavior of **1-Fe*o*Cp** and **2-FeN*** upon thermal treatment with hydrogen and propane in turn.

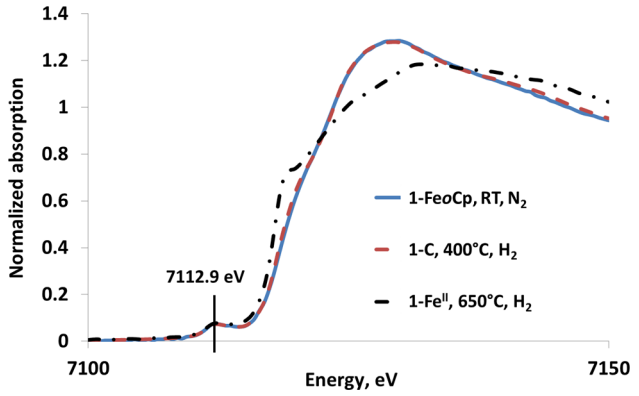

Figure 3. X-ray absorption near-edge structure spectroscopy (XANES) of **1-Fe*o*Cp**, **1-C** and **1-Fe^{II}**. The pre-edge of the XANES used to identify the formal oxidation state is marked with the vertical line.

The local Fe coordination was determined by EXAFS, which provides information about the number of neighboring atoms and the average bond distance. Scattering is proportional to the number of electrons in the neighboring atom; thus, C and O scatters cannot be distinguished by this method. A first-shell Fe−X (X = O or C) peak was observed in the magnitude of the Fourier transform (FT) of the EXAFS data for **1-Fe*o*Cp** (Figure 4) and is the average of the Fe−X from the support and remaining Fe-pentadienyl ligand. Figure 4 shows the magnitude

DOI: 10.1021/acscatal.5b00248
ACS Catal. 2015, 5, 3494−3503

Table 1. XANES and EXAFS Data of Fe(*o*Cp)$_2$ Precursor, Isolated Fe/SiO$_2$ Catalysts, Fe Nanoparticle Catalysts, and Fe Oxide Cluster Catalysts

sample	treatment	pre-edge energy, keV	oxidation state	scatter	*N*	*R*, Å	$\Delta\sigma^2$ ($\times 10^3$)	ΔE_0, eV
Fe(*o*Cp)$_2$	catalyst precursor	7.1130	2+	Fe−C	10.0	2.00	6.0	5.0
Fe/SiO$_2$ (Fe(*o*Cp)$_2$)	as prepared, **1-Fe*o*Cp**	7.1129	2+	Fe−O/C	3.7	1.96	8.0	2.0
	H$_2$ 400 °C, RT **1-C**	7.1128	2+	Fe−O	4.3	1.95	6.0	1.0
	H$_2$, 650 °C, RT, **1-Fe^{II}**	7.1130	2+	Fe−O	2.9	1.82	4.0	0.8
	C$_3$H$_8$, 650 °C, RT, **1-Fe^{II}**	7.1129	2+	Fe−O	2.9	1.85	8.0	2.1
Fe NPs/SiO$_2$ (Fe[N(SiMe$_3$)$_2$]$_2$)	as prepared, **2-FeN***	7.1129	2+	Fe−O/N	3.1	1.98	4.0	0.6
	H$_2$, 650 °C, RT, **2-NP-Fe^0**	7.1120[a]	0	Fe−Fe	7.2	2.47	1.0	−1.8
FeO$_x$ cluster/SiO$_2$ IWI	air, RT	7.1144	3+	Fe−O	6.1	1.92	9.0	−3.9
	H$_2$, 650 °C, RT	7.1128	2+	Fe−O	3.9	1.91	9.0	−0.7
Fe(III) ZSM-5	air, RT	7.1145	3+	Fe−O	4.1	1.84	8.0	−2.4

[a]7.1120 keV is the edge energy of Fe^0 nanoparticles, no pre-edge energy feature can be obtained from Fe in zerovalent state.

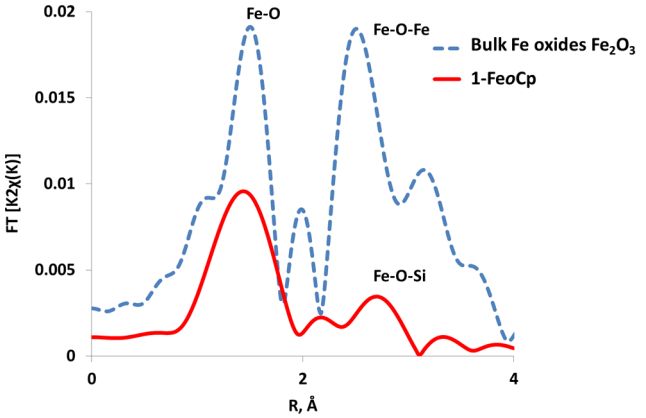

Figure 4. Magnitude of the Fourier transforms of the EXAFS spectra of **1-Fe*o*Cp** and bulk Fe$_2$O$_3$ standard.

of the FT of **1-Fe*o*Cp** in comparison with bulk Fe$_2$O$_3$, which has 6 Fe−O bonds at average distance of ∼1.99 Å. The position of the first shell peak of **1-Fe*o*Cp** is similar to that of Fe(III) oxide, but the smaller peaks are consistent with fewer neighbors.

Fitting of the Fe−X first shell peak with the phase and amplitude functions prepared from reference compounds, for example, Fe(acac)$_3$, 6 Fe−O at 1.99 Å (where acac is acetylactetonate), **1-Fe*o*Cp** has four Fe−X (X = O or C) neighbors at an average bond distance of 1.96 Å. Determination of the precise coordination geometry of the ligand to Fe is not possible; however, the low total coordination number of the complex indicates that the pentadienide ligand is not η^5-bonded in the supported complex as it is in the precursor (Scheme 1).

In addition to the Fe−X (X = O or C) coordination shell, there is also a small, higher shell peak at ∼2.5 Å due to scattering by C atoms from the pentadienide ligand and support at longer distances. This peak is much smaller and at a distance different from that of Fe(III) oxide, suggesting that these grafted Fe sites are monomolecular, that is, an isolated site. The remaining pentadienide ligand was removed from **1-Fe*o*Cp** by heating to 400 °C in H$_2$ (Scheme 3). The product (**1-C**) was analyzed by infrared and the disappearance of the C−H stretching bands was observed (Figure 5, bottom). The thermal removal of diene ligand could be due to the reaction between the pentadienide ligand and the surface bridging hydroxyl, resulting in a new Fe−O bond and a free *o*CpH or by reaction with H$_2$. Regardless, an increase in the isolated OH stretching resonance at 3740 cm^{-1} is observed (Figure 5, bottom).

A final possible mechanism for removal of *o*CpH could be hydrolysis of the organic ligand by H$_2$O, which is generated by thermal dehydration of surface hydroxyls at evaluated temperatures. The XANES pre-edge energy is 7112.8 eV, indicating that the oxidation state remains Fe^{II} under H$_2$ at 400 °C. Fitting of the EXAFS spectra gives four Fe−O bonds at a distance of 1.95 Å (Table 1). The Fe−O bond distance in bulk iron oxides is generally >1.90 Å[46−49] (see Table S2), which suggests the formation of small iron oxides cluster (**1-C**). This is not surprising because we have observed that crystalline FeOx can be grown by atomic layer deposition (ALD) in previous work with the Fe(*o*Cp)$_2$ precursor.[42]

Further evolution of the surface iron species occurs at a higher temperature (650 °C) in hydrogen, although the oxidation state of Fe remains 2+ with a pre-edge energy of

Scheme 3. Transformation of Surface Fe Species in H$_2$ at Evaluated Temperature To Form 1-Fe^{II}

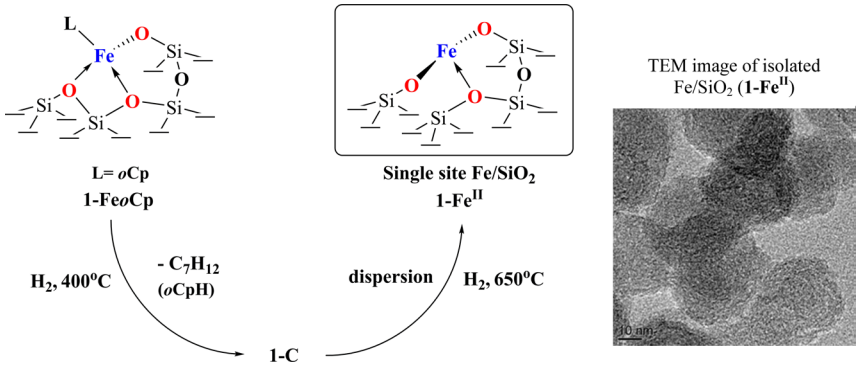

DOI: 10.1021/acscatal.5b00248
ACS Catal. 2015, 5, 3494−3503

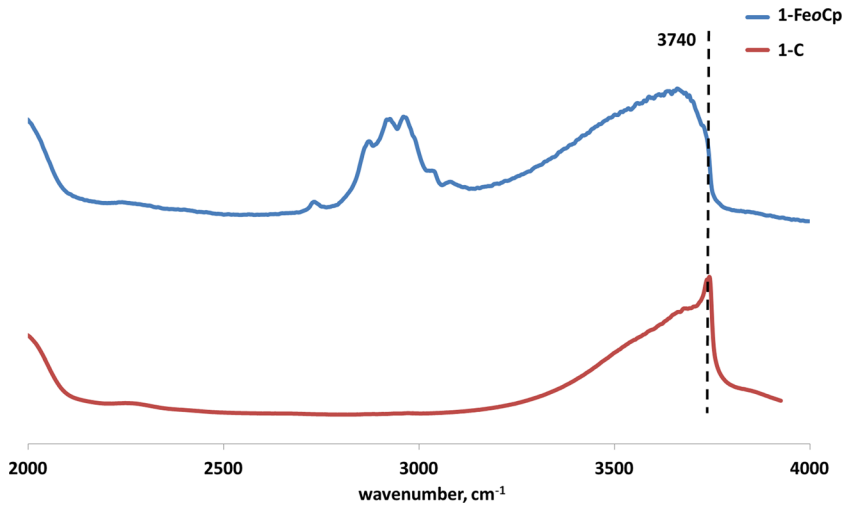

Figure 5. DRIFTS spectra of **1-FeoCp** (top) and **1-C** (bottom).

7113.0 eV (Scheme 3). The shape of the XANES is different from that at 400 °C (Figure 3), indicating another change in the Fe surface structure. The fit of the EXAFS first-shell peak indicates that there are 3 Fe−O bonds at 1.82 Å to form the isolated Fe^{II}/SiO_2 complex **1-Fe^{II}** (Figure 6). There is a

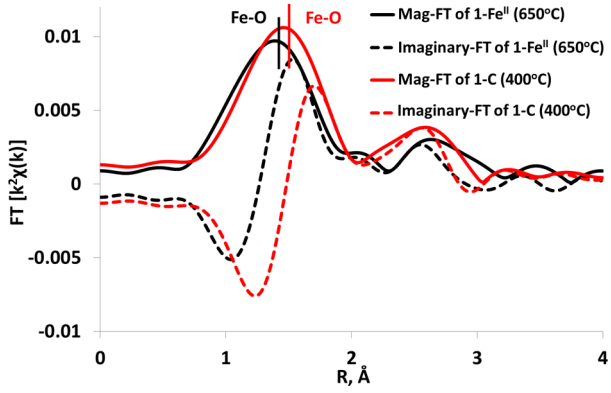

Figure 6. Fourier-transformed k^2-weighted EXAFS spectra of **1-Fe^{II}** (Δk = 2.93−10.05) (650 °C) and **1-C** (Δk = 2.66−10.21) (400 °C).

decrease in the magnitude FT of **1-Fe^{II}** when comparing it with **1-C**. That decrease is consistent with loss of 1 Fe−O and a shift to lower R, which is consistent with the shorter Fe−O bond distance at 650 °C. Importantly, there is no indication of metallic Fe in the XANES or EXAFS spectrum after 650 °C treatment with hydrogen or propane.

High-temperature dispersion of supported transition metal oxides has previously been reported for Co,[14] Ni,[50] Mo,[51,52] V,[53] and Cr.[54] For the case of this study, the synthesis of **1-FeoCp** is self-controlled in terms of Fe loading because the excess precursor does not readily react with surface hydroxyls because of the steric bulk of the diene ligand. As a result, the total loading of Fe is far lower than the monolayer concentration. Thus, redispersion at high temperature (650 °C) is more likely to form isolated Fe(II) surface species. At higher Fe loadings, typical of the incipient wetness impregnation method in which the saturation or oversaturation of the surface hydroxyl is reached, the same Fe(II) silicate species are not formed.

Although the higher shell peak in EXAFS of the **1-Fe^{II}** at 650 °C is small, as shown in Figure 6, it is difficult to get a reliable fit to differentiate whether this is from Fe−O−Si or Fe−O−Fe. Therefore, the EXAFS spectrum was also obtained for Fe-MFI, that is, isolated Fe in the ZSM-5 structure for comparison. In the Fe-MFI framework, Fe has a tetrahedral geometry with four Fe−O bonds in the zeolite framework, which is similar to AlO_4^- in ZMS-5, and its higher shell peak corresponds to Fe−O−Si. A fit of the first shell peak in FT indicates that there are four Fe−O bonds at 1.84 Å, which is shorter than that in Fe oxides and is similar to that for the **1-Fe^{II}** treated at 650 °C. The similarity of the Fe−O bond distances in **1-Fe^{II}** and Fe-MFI suggests that the second shell neighbor is Si, rather than Fe. The higher shell peak of Fe-MFI is also small and is at a distance similar to that of the higher shell peak in **1-Fe^{II}**, which is consistent with bonding of the Fe to the silica surface.

In contrast to the chemical transformation observed to form **1-Fe^{II}** at evaluated temperature, thermal treatments of Fe/SiO_2 derived from $Fe[N(SiMe_3)_2]_2$ (**2-FeN***) follow a drastically different path. EXAFS shows that **2-FeN*** is a three-coordinate Fe^{II} with an average bond distance of 1.98 Å (Table 1). The lower coordination number is noteworthy and may be a result of the concomitant formation of $Si-O-SiMe_3$ groups when synthesizing **2-FeN***; however, this remains a hypothesis at this time. Upon treatment of **2-FeN*** with H_2 at 650 °C, the Fe^{II} reduced to metallic Fe^0 nanoparticles (**2-NP-Fe^0**). The XANES of **2-FeN*** after H_2 treatment at 650 °C clearly shows the shift to the metallic energy (7112.0 eV) and shape of the XANES (Figure 7a).

To the best of our knowledge this is the first report of controlled synthesis of metallic iron nanoparticles on silica, by reducing surface-grafted Fe species at relatively low temperature, although $Fe[N(SiMe_3)_2]_2$ has been shown to reduce to metallic iron in solution by Chaudret et al.[55] The EXAFS of **2-NP-Fe^0** is also significantly different from that of **2-FeN***, as shown in Figure 7b. The EXAFS fit gives an Fe−Fe coordination number of 7.2 at 2.47 Å (metallic Fe foil has a coordination number of 8 (BCC) at a distance of 2.48 Å). The slightly lower coordination number of **2-NP-Fe^0** than bulk metal is commonly observed in nanoparticles because a significant portion of the metal atoms are surface atoms and have a lower coordination number than the bulk material. Such surface transformation of **2-FeN*** is shown in Scheme 4.

DOI: 10.1021/acscatal.5b00248
ACS Catal. 2015, 5, 3494−3503

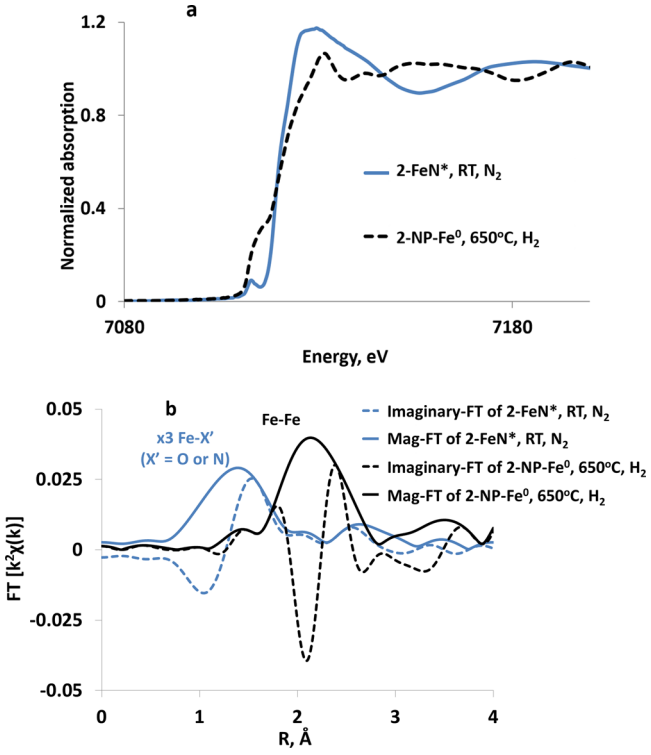

Figure 7. (a) XANES spectra and (b) Fourier-transformed k^2-weighted EXAFS spectra of **2-FeN*** (Δk = 2.85−10.58) and **2-NP-Fe^0** (Δk = 2.49−11.58).

Scheme 4. Transformation of Surface Fe Species 2-FeN* in H_2 at Evaluated Temperature To Form 2-NP-Fe^0 and TEM Image Showing Iron Nanoparticles

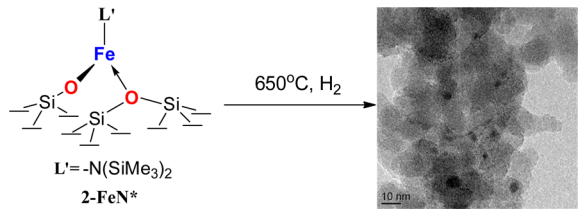

Transmission electron microscopy (TEM) of **2-NP-Fe^0** enabled a size distribution analysis of **2-NP-Fe^0**, Figure 8. The average size of the nanoparticles in **2-NP-Fe^0** is 3 nm ±0.7 nm, and the distribution of the particle sizes is relatively narrow. We have not attempted to optimize the synthesis of **2-NP-Fe^0**.

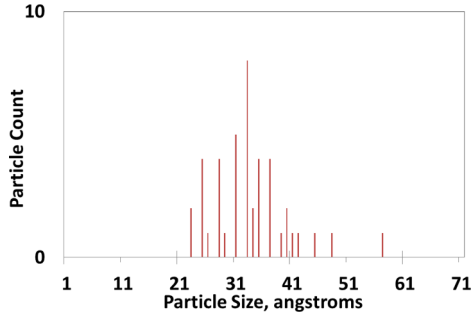

Figure 8. Silica-supported Fe nanoparticle size distribution was determined by TEM (Scheme 4).

Finally, conventional iron oxide nanoparticles on silica were prepared by incipient wetness impregnation of $Fe(NO_3)_3 \cdot 9H_2O$, followed by calcination at 300 °C. The XANES pre-edge energy (7114.4 eV, Table 1) is consistent with Fe(III). The fit of the first shell Fe−O indicates there are 6 bonds at 1.92 Å. In H_2 at 650 °C, the iron oxide is reduced to Fe(II), and there are four Fe−O bonds at 1.91 Å. The higher shell peak in this catalyst (Figure S2), however, is small, indicating small Fe(III) and Fe(II) oxide clusters in air at RT and in H_2 at 650 °C, respectively.

Catalytic Performance for Propane Dehydrogenation. All of the Fe/SiO_2 materials were evaluated for propane dehydrogenation in a continuous flow, fixed-bed reactor. The experimental details of the catalyst testing are given in the Experimental section. Because the thermodynamic equilibrium for propene is favored at high temperature, the reaction was conducted at 650 °C, where equilibrium conversion is ~70%.[11,56] At temperatures above 600 °C, thermal cracking also contributes to the observed conversion under our conditions. Therefore, the catalytic conversion and selectivity were determined by subtracting the background thermal cracking from that obtained with the catalyst, that is, thermal plus catalytic conversion.

Catalytic tests of **1-Fe^{II}** were performed under differential conversions of <10% (5%) initially to determine intrinsic rates at t = 0 h. The turnover frequency (TOF, h^{-1}), for example, the molecules of propane converted per hour per Fe ion, was calculated by assuming all Fe is active. The TOF as a function of time of isolated **1-Fe^{II}** is shown in Figure 9 and is 1.1 h^{-1} (or 3.1 × 10^{-4} s^{-1}) at t = 0 h. The catalyst is stable during an 18 h test, with the rate increasing slightly to 1.4 h^{-1} (or 3.9 × 10^{-4} s^{-1}) over this period (Table 2). Such catalytic rates are similar to most other known first-row transition metal oxide dehydrogenation catalysts (Cr, Ga, V, etc.).[11] The catalytic selectivity for propene was initially high (>99%), and it

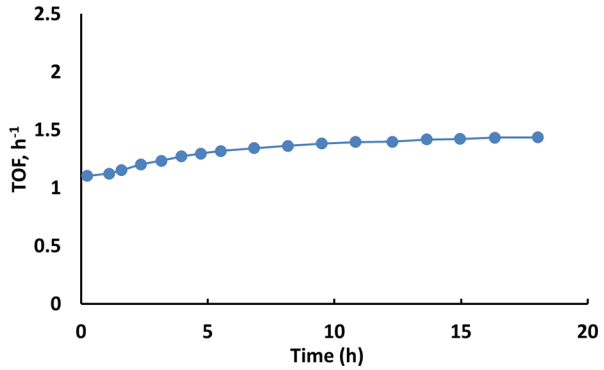

Figure 9. TOF of **1-Fe^{II}** as a function of time.

Table 2. TOF and Propene Selectivity of Silica Supported Fe Catalysts

	C_3H_8 dehydrogenation TOF (h^{-1})		conversion (%)		selectivity to C_3H_6	
catalyst	t = 0 h	t = 18 h	t = 0 h	t = 18 h	t = 0 h	t = 18 h
1-Fe^{II}	1.1	1.4	4.9	6.3	>99%	
2-NP-Fe^0	43		27[a]		14%	

[a]0.5 g of catalyst was utilized for propane dehydrogenation.

DOI: 10.1021/acscatal.5b00248
ACS Catal. 2015, 5, 3494−3503

remained at such high selectivity over 18 h. However, the overall propene selectivity (thermal cracking + catalytic dehydrogenation) was ~70%, as shown in Figure S5, which is due to the highly unselective nature of thermal cracking. The XANES, Figure S2, and EXAFS spectra were also obtained at propane dehydrogenation reaction conditions and after cooling to room temperature. Both spectra were identical to that in H_2, showing only low-coordinate Fe(II) silicate species (see fits in Table 1).

Although the XANES and EXAFS spectra suggest that the **1-Fe^{II}** is a well-defined, low-coordinate Fe(II) bound directly to the silica surface, there may be small amounts of metallic Fe or iron oxide nanoparticles that could have much higher rates and are responsible for the catalytic activity. Therefore, comparisons of **1-Fe^{II}** with **2-NP-Fe^0** and iron oxide particles were performed..

At t = 0 h, the TOF for conversion of propane of the metallic **2-NP-Fe^0** was high, almost 40 times higher than that of **1-Fe^{II}**. Although highly active in consuming propane, **2-NP-Fe^0** produces little propene. Only 14% of the product is propene, with the remainder of the gaseous products being methane and ethene. TEM micrographs of the spent catalyst showed metallic Fe NPs with carbon nanotubes formed during the propane dehydrogenation reaction (Scheme 5).

Scheme 5. Formation of Carbon Nanotubes under Propane Dehydrogenation Conditions by 2-NP-Fe^0

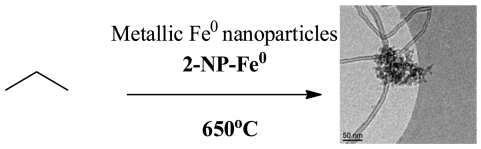

Silica-supported Fe(II) oxide clusters were poorly active. Little conversion of propane was observed with the same amount of iron as in the tests of **1-Fe^{II}**. At the very low catalytic and high thermal propane conversions (cracking), it was not possible to accurately determine the TOF, product selectivity, or rate of deactivation of the Fe(II) oxide clusters. As a result of these comparisons, we conclude that single-site, three-coordinate Fe^{II} is the catalytically active and selective species. Similar propane dehydrogenation activity of isolated Fe in zeolite was also reported by Lobo et al.[37]

Although homogeneous catalysts are not thermally stable at propane dehydrogenation temperature, catalytic olefin hydrogenation, which is the microscopic reverse reaction to alkane dehydrogenation, has been studied in some detail in homogeneous systems. Catalytic hydrogenation is normally proposed to occur by an oxidative addition and reductive elimination pathway for late transition metals, Wilkinson's catalyst $RhCl(PPh_3)_3$ being one of the most-studied examples. In this case, oxidative addition of H_2 forms a Rh^{III} dihydride intermediate $Rh(H)_2Cl(PPh_3)_2$.[57,58] Oxidative addition is less known in first-row systems. However, the tris-(diisopropylphosphino)borate–supported Fe^{II} system studied by Daida and Peters was found to form Fe$^{IV}(H)_x$ intermediates when observed by ^{1}H NMR spectroscopy. On the basis of observed Fe^{II}/Fe^{IV} redox chemistry, the authors proposed a metal-redox pathway over alternative, nonredox mechanisms.[59] In contrast, the bis(imino)pyridine iron complexes synthesized by Chirik et al. are highly efficient olefin hydrogenation catalysts under mild conditions[60−63] but do not appear to change their formal oxidation state during catalysis. One complication is the propensity of the ligand to undergo redox activity, although it is an open question whether the redox potentials of the ligand are within the energy regime necessary for catalysis. Our isolated Fe catalyst **1-Fe^{II}** also does not appear to change oxidation state in either hydrogen or propane under reaction conditions, in contrast to the Peters system. In addition, there is no evidence that SiO_2 is capable of redox behavior, and electron transfer between the metal center and support is unlikely in this case. Therefore, we favor a nonredox, heterolytic cleavage mechanism for propane dehydrogenation, in analogy with other silica-supported systems that we have recently reported.[13,14]

We propose two possible non-redox mechanisms for the dehydrogenation chemistry shown by **1-Fe^{II}** (Figure 10). The

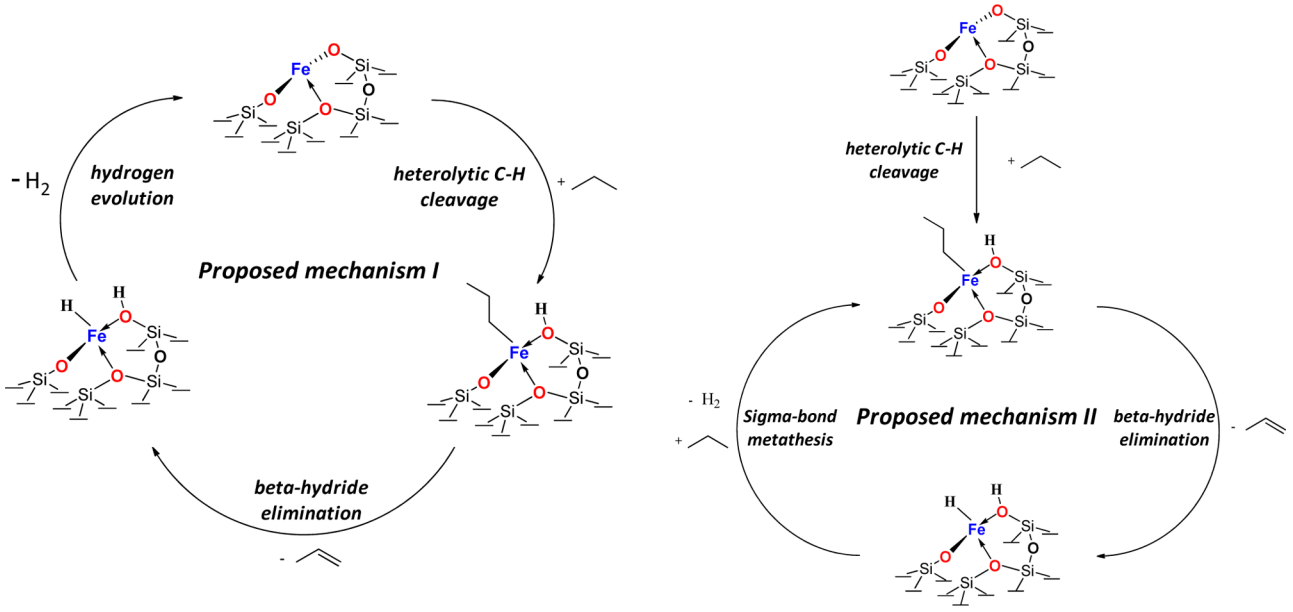

Figure 10. Two proposed reaction mechanisms of propane dehydrogenation by isolated Fe/SiO_2 (**1-Fe^{II}**).

DOI: 10.1021/acscatal.5b00248
ACS Catal. 2015, 5, 3494−3503

initial step of both proposed mechanisms consists of heterolytic C−H cleavage to form a metal alkyl and a ≡SiOH, that is, a protonated Fe−O−Si bond. This is followed by a rapid β-hydride elimination of the Fe alkyl to release propene. However, the subsequent reaction of the resulting iron hydride could pass through two potential pathways: reaction of the iron hydride with H^+ on ≡SiOH to form hydrogen and regenerate a three-coordinate Fe or direct reaction of the Fe−H with propane through σ-bond metathesis to form hydrogen and an iron propyl. σ Bond metathesis reactivity had been reported for late transition metal hydrides; for example, the ruthenium complex $TpRu(PPh_3)(CH_3CN)H$ (Tp = hydrotris(pyrazolyl)-borate) catalyzed H/D exchange between alkanes.[64,65] Peters and Daida et al.[59] also proposed the σ bond metathesis pathway for their $[PhBP^{iPr}_3]Fe-R$ system but discounted it on the basis of the observable Fe^{IV} intermediates and the isolation of other Fe^{IV} complexes, as noted above. A related cobalt(II) alkyl supported by the tridentate ligand bis[2-(dicyclohexylphosphino)ethyl]amine was also proposed by Hanson et al. to react with hydrogen via σ bond metathesis to form a cobalt hydride and form the catalytically active hydrogenation intermediate.[66,67] The reactivity of surface-bound Fe hydrides, which is believed to be a critical reaction intermediate for alkane activation, is a topic of continuing research in our group.

Heterolytic cleavage of C−H bonds has also been suggested by Weckhuysen et al.[68] and Copéret[69] to be the activation mechanism of ethane dehydrogenation by Cr/Al_2O_3. Copéret[69] also proposes heterolytic cleavage as the initiation step in the Cr/SiO_2 Phillips catalyst.[70,71] For catalysts proceeding through this mechanism, midtransition metals with partially occupied d shells should have a lower barrier to beta hydride elimination, which is the rate-determining step for Zn[11,13] and Ga-based[12] catalysts. However, the lower Lewis acidity of the transition metals may mitigate the advantages gained in the lowering of the barrier to β-hydride elimination. As a result, tuning the coordination environment of surface-bound, well-defined transition metals is key to developing new catalysts for C−H activation based upon robust heterogeneous supports with well-defined catalyst species. The results reported here suggest that such catalysts can be prepared if proper understanding of the surface species and control over their structure can be achieved.

CONCLUSION

Isolated Fe^{II}/SiO_2 (**1-Fe^{II}**) was prepared by surface organometallic chemistry with $Fe(oCp)_2$ precursor and high temperature (650 °C) treatment in hydrogen. The resulting isolated Fe^{II} is a highly active and stable catalyst for propane dehydrogenation with high selectivity of propene. A three-coordinate Fe^{II} was confirmed to be the catalytically active species by in situ XANES and EXAFS. Other possible active species, such as metallic Fe(0) and $Fe^{II}O_X$ nanoparticles, were prepared and shown not to be catalytically competent catalysts. They showed low selectivity or low activity compared with **1-Fe^{II}**. A non-redox mechanism for propane dehydrogenation is proposed on the basis of other high-temperature catalysts supported by hard oxide ligands. Synthesis of other low-coordinate transition metal catalysts and their catalytic performances is under investigation.

ASSOCIATED CONTENT

Supporting Information

The following file is available free of charge on the ACS Publications website at DOI: 10.1021/acscatal.5b00248.

Additional spectra and experimental details (PDF)

AUTHOR INFORMATION

Corresponding Authors

*E-mail: ahock@iit.edu or hock@anl.gov.

*E-mail: millerjt@anl.gov.

Notes

The authors declare no competing financial interest.

ACKNOWLEDGMENTS

The work was supported by the U.S. Department of Energy, Office of Basic Energy Sciences, Chemical Sciences under Contract DE-AC-02-06CH11357. B.H. and A.S.H. would like to thank the Illinois Institute of Technology for a Starr-Fieldhouse Fellowship (BH) and startup funding support. Use of the Advanced Photon Source is supported by the U.S. Department of Energy, Office of Science, and Office of Basic Energy Sciences, under Contract DE-AC02-06CH11357. Materials Research Collaborative Access Team (MRCAT, Sectors 10-BM and 10-ID) operations are supported by the Department of Energy and the MRCAT member institutions.

REFERENCES

(1) Nakagawa, K.; Kajita, C.; Ide, Y.; Okamura, M.; Kato, S.; Kasuya, H.; Ikenaga, N.; Kobayashi, T.; Suzuki, T. *Catal. Lett.* **2000**, *64*, 215−221.

(2) Michorczyk, P.; Ogonowski, J. *Appl. Catal., A* **2003**, *251*, 425−433.

(3) Michorczyk, P.; Gora-Marek, K.; Ogonowski, J. *Catal. Lett.* **2006**, *109*, 195−198.

(4) Nakagawa, K.; Okamura, M.; Ikenaga, N.; Suzuki, T.; Kobayashi, T. *Chem. Commun.* **1998**, 1025−1026.

(5) Biscardi, J. A.; Iglesia, E. *Phys. Chem. Chem. Phys.* **1999**, *1*, 5753−5759.

(6) Biscardi, J. A.; Iglesia, E. *Catal. Today* **1996**, *31*, 207−231.

(7) Yu, S. Y.; Yu, G. J.; Li, W.; Iglesia, E. *J. Phys. Chem. B* **2002**, *106*, 4714−4720.

(8) Li, W.; Yu, S. Y.; Meitzner, G. D.; Iglesia, E. *J. Phys. Chem. B* **2001**, *105*, 1176−1184.

(9) Al-Yassir, N.; Akhtar, M. N.; Al-Khattaf, S. *J. Porous Mater.* **2012**, *19*, 943−960.

(10) Thomas, J. M.; Liu, X. S. *J. Phys. Chem.* **1986**, *90*, 4843−4847.

(11) Sattler, J. J. H. B.; Ruiz-Martinez, J.; Santillan-Jimenez, E.; Weckhuysen, B. M. *Chem. Rev.* **2014**, *114*, 10613−10653.

(12) Fricke, R.; Kosslick, H.; Lischke, G.; Richter, M. *Chem. Rev.* **2000**, *100*, 2303−2406.

(13) Schweitzer, N. M.; Hu, B.; Das, U.; Kim, H.; Greeley, J.; Curtiss, L. A.; Stair, P. C.; Miller, J. T.; Hock, A. S. *ACS Catal.* **2014**, *4*, 1091−1098.

(14) Hu, B.; "Bean" Getsoian, A.; Schweitzer, N. M.; Das, U.; Kim, H.; Niklas, J.; Poluektov, O.; Curtiss, L. A.; Stair, P. C.; Miller, J. T.; Hock, A. S. *J. Catal.* **2015**, *322*, 24−37.

(15) Trofimenko, S. *Scorpionates: The Coordination Chemistry of Polypyrazolylborate Ligands*; Imperial College Press: London, 1999.

(16) Figueroa, J. S.; Melnick, J. G.; Parkin, G. *Inorg. Chem.* **2006**, *45*, 7056−7058.

(17) Sánchez-Barba, L. F.; Garcés, A. s.; Fernández-Baeza, J.; Otero, A.; Alonso-Moreno, C.; Lara-Sánchez, A. n.; Rodríguez, A. M. *Organometallics* **2011**, *30*, 2775−2789.

(18) Sazama, G. T.; Betley, T. A. *Inorg. Chem.* **2010**, *49*, 2512−2524.

DOI: 10.1021/acscatal.5b00248
ACS Catal. 2015, 5, 3494−3503

(19) Jernigan, F. E.; Sieracki, N. A.; Taylor, M. T.; Jenkins, A. S.; Engel, S. E.; Rowe, B. W.; Jové, F. A.; Yap, G. P. A.; Papish, E. T.; Ferrence, G. M. *Inorg. Chem.* **2006**, *46*, 360−362.
(20) Pullen, E. E.; Rabinovich, D.; Incarvito, C. D.; Concolino, T. E.; Rheingold, A. L. *Inorg. Chem.* **2000**, *39*, 1561−1567.
(21) Sánchez-Barba, L. F.; Garcés, A.; Fajardo, M.; Alonso-Moreno, C.; Fernández-Baeza, J.; Otero, A.; Antiñolo, A.; Tejeda, J.; Lara-Sánchez, A.; López-Solera, M. I. *Organometallics* **2007**, *26*, 6403−6411.
(22) Yang, X. F.; Wang, A. Q.; Qiao, B. T.; Li, J.; Liu, J. Y.; Zhang, T. *Acc. Chem. Res.* **2013**, *46*, 1740−1748.
(23) Gajan, D.; Coperet, C. *New J. Chem.* **2011**, *35*, 2403−2408.
(24) Coperet, C.; Chabanas, M.; Saint-Arroman, R. P.; Basset, J. M. *Angew. Chem., Int. Ed.* **2003**, *42*, 156−181.
(25) Thomas, J. M.; Raja, R.; Lewis, D. W. *Angew. Chem., Int. Ed.* **2005**, *44*, 6456−6482.
(26) Marks, T. J. *Acc. Chem. Res.* **1992**, *25*, 57−65.
(27) Wegener, S. L.; Marks, T. J.; Stair, P. C. *Acc. Chem. Res.* **2012**, *45*, 206−214.
(28) Conley, M. P.; Mougel, V.; Peryshkov, D. V.; Forrest, W. P.; Gajan, D.; Lesage, A.; Emsley, L.; Coperet, C.; Schrock, R. R. *J. Am. Chem. Soc.* **2013**, *135*, 19068−19070.
(29) Rascon, F.; Coperet, C. *J. Organomet. Chem.* **2011**, *696*, 4121−4131.
(30) Blanc, F.; Thivolle-Cazat, J.; Basset, J. M.; Coperet, C.; Hock, A. S.; Tonzetich, Z. J.; Schrock, R. R. *J. Am. Chem. Soc.* **2007**, *129*, 1044−1045.
(31) Nozaki, C.; Lugmair, C. G.; Bell, A. T.; Tilley, T. D. *J. Am. Chem. Soc.* **2002**, *124*, 13194−13203.
(32) Fujdala, K. L.; Brutchey, R. L.; Tilley, T. D. In *Topics in Organometallic Chemistry*; Copéret, C., Chaudret, B., Eds.; Springer: Berlin/Heidelberg, 2005; Vol. *16*, pp 69−115.
(33) Brutchey, R. L.; Ruddy, D. A.; Andersen, L. K.; Tilley, T. D. *Langmuir* **2005**, *21*, 9576−9583.
(34) Fujdala, K. L.; Tilley, T. D. *J. Catal.* **2003**, *216*, 265−275.
(35) Tilley, T. D. *J. Mol. Catal. A: Chem.* **2002**, *182*−*183*, 17−24.
(36) Prieto-Centurion, D.; Notestein, J. M. *J. Catal.* **2011**, *279*, 103−110.
(37) Yun, J. H.; Lobo, R. F. *J. Catal.* **2014**, *312*, 263−270.
(38) Rangus, M.; Mazaj, M.; Dražić, G.; Popova, M.; Tušar, N. *Materials* **2014**, *7*, 4243−4257.
(39) Popova, M.; Ristić, A.; Lazar, K.; Maučec, D.; Vassileva, M.; Novak Tušar, N. *ChemCatChem* **2013**, *5*, 986−993.
(40) Wilson, D. R.; Dilullo, A. A.; Ernst, R. D. *J. Am. Chem. Soc.* **1980**, *102*, 5928−5930.
(41) Wilson, D. R.; Ernst, R. D.; Cymbaluk, T. H. *Organometallics* **1983**, *2*, 1220−1228.
(42) Riha, S. C.; Racowski, J. M.; Lanci, M. P.; Klug, J. A.; Hock, A. S.; Martinson, A. B. F. *Langmuir* **2013**, *29*, 3439−3445.
(43) Olmstead, M. M.; Power, P. P.; Shoner, S. C. *Inorg. Chem.* **1991**, *30*, 2547−2551.
(44) Wilson, D. R.; DiLullo, A. A.; Ernst, R. D. *J. Am. Chem. Soc.* **1980**, *102*, 5928−5930.
(45) Andersen, R. A.; Faegri, K.; Green, J. C.; Haaland, A.; Lappert, M. F.; Leung, W. P.; Rypdal, K. *Inorg. Chem.* **1988**, *27*, 1782−1786.
(46) Kaneko, K.; Kosugi, N.; Kuroda, H. *J. Chem. Soc., Faraday Trans. 1* **1989**, *85*, 869−881.
(47) Corrias, A.; Ennas, G.; Mountjoy, G.; Paschina, G. *Phys. Chem. Chem. Phys.* **2000**, *2*, 1045−1050.
(48) Wu, Z. Y.; Gota, S.; Jollet, F.; Pollak, M.; Gautier-Soyer, M.; Natoli, C. R. *Phys. Rev. B: Condens. Matter Mater. Phys.* **1997**, *55*, 2570−2577.
(49) Pauling, L.; Hendricks, S. B. *J. Am. Chem. Soc.* **1925**, *47*, 781−790.
(50) Nakayama, T.; Arai, M.; Nishiyama, Y. *J. Catal.* **1984**, *87*, 108−115.
(51) Braun, S.; Appel, L. G.; Camorim, V. L.; Schmal, M. *J. Phys. Chem. B* **2000**, *104*, 6584−6590.
(52) Collart, O.; Van der Voort, P.; Vansant, E. F.; Gustin, E.; Bouwen, A.; Schoemaker, D.; Rao, R. R.; Weckhuysen, B. M.; Schoonheydt, R. A. *Phys. Chem. Chem. Phys.* **1999**, *1*, 4099−4104.
(53) Hess, C. *J. Catal.* **2007**, *248*, 120−123.
(54) Liu, Y. H.; Chaoran, H.; Pei, R.; Xie, Y.; Tang, Y. *Acta Phys. Chim. Sin.* **1988**, *4*, 376−381.
(55) Kelsen, V.; Wendt, B.; Werkmeister, S.; Junge, K.; Beller, M.; Chaudret, B. *Chem. Commun.* **2013**, *49*, 3416−3418.
(56) Weckhuysen, B. M.; Schoonheydt, R. A. *Catal. Today* **1999**, *51*, 223−232.
(57) Halpern, J.; Wong, C. S. *J. Chem. Soc., Chem. Commun.* **1973**, 629−630.
(58) Tolman, C. A.; Meakin, P. Z.; Lindner, D. L.; Jesson, J. P. *J. Am. Chem. Soc.* **1974**, *96*, 2762−2774.
(59) Daida, E. J.; Peters, J. C. *Inorg. Chem.* **2004**, *43*, 7474−7485.
(60) Knijnenburg, Q.; Gambarotta, S.; Budzelaar, P. H. M. *Dalton Trans.* **2006**, 5442−5448.
(61) Bart, S. C.; Lobkovsky, E.; Chirik, P. J. *J. Am. Chem. Soc.* **2004**, *126*, 13794−13807.
(62) Bart, S. C.; Chlopek, K.; Bill, E.; Bouwkamp, M. W.; Lobkovsky, E.; Neese, F.; Wieghardt, K.; Chirik, P. J. *J. Am. Chem. Soc.* **2006**, *128*, 13901−13912.
(63) Bart, S. C.; Lobkovsky, E.; Bill, E.; Chirik, P. J. *J. Am. Chem. Soc.* **2006**, *128*, 5302−5303.
(64) Ng, S. M.; Lam, W. H.; Mak, C. C.; Tsang, C. W.; Jia, G. C.; Lin, Z. Y.; Lau, C. P. *Organometallics* **2003**, *22*, 641−651.
(65) Lam, W. H.; Jia, G. C.; Lin, Z. Y.; Lau, C. P.; Eisenstein, O. *Chem. - Eur. J.* **2003**, *9*, 2775−2782.
(66) Zhang, G. Q.; Vasudevan, K. V.; Scott, B. L.; Hanson, S. K. *J. Am. Chem. Soc.* **2013**, *135*, 8668−8681.
(67) Zhang, G. Q.; Scott, B. L.; Hanson, S. K. *Angew. Chem., Int. Ed.* **2012**, *51*, 12102−12106.
(68) Olsbye, U.; Virnovskaia, A.; Prytz, O.; Tinnemans, S. J.; Weckhuysen, B. M. *Catal. Lett.* **2005**, *103*, 143−148.
(69) Conley, M. P.; Delley, M. F.; Núñez-Zarur, F.; Comas-Vives, A.; Copéret, C. *Inorg. Chem.* **2015**, DOI: 10.1021/ic502696n.
(70) Delley, M. F.; Núñez-Zarur, F.; Conley, M. P.; Comas-Vives, A.; Siddiqi, G.; Norsic, S.; Monteil, V.; Safonova, O. V.; Copéret, C. *Proc. Natl. Acad. Sci. U. S. A.* **2014**, *111*, 11624−11629.
(71) Conley, M. P.; Delley, M. F.; Siddiqi, G.; Lapadula, G.; Norsic, S.; Monteil, V.; Safonova, O. V.; Copéret, C. *Angew. Chem., Int. Ed.* **2014**, *53*, 1872−1876.

DOI: 10.1021/acscatal.5b00248
ACS Catal. 2015, 5, 3494−3503